ADVANCED SENSOR RESEARCH Open Access
www.advsensorres.com

Organic Transistor-Based Biosensors for Viral RNA Detection and Variant Monitoring: From SARS-CoV-2 to Effective Management of Future Pandemics

Stefano Lai, Roberto Cusano, Alessandra Scano, Giorgio Fotia, and Annalisa Bonfiglio*

The COVID-19 crisis has defined the need of novel approaches for a straightforward management of pandemic and epidemic conditions. Here, an approach based on electronic sensing of viral RNA is proposed for both virus detection and variant tracking. The sensing strategy of the Organic Charge-Modulated Field-Effect Transistor (OCMFET) is employed for the development of a multi-sensing platform, capable of parallel evaluation of control references and investigated samples. PCR-free detection of viral genomic RNA is demonstrated at different target concentrations, with optimal discrimination with respect to negative control. Moreover, the same approach is feasible for virus variant tracking, as a screening strategy for mutation detection in PCR-amplified samples: the approach can be used for a rationalization of RNA sequencing procedures, which are difficult to perform in the acute phases of pandemics, but are fundamental for an effective pandemic management. The results pave the way for novel strategies to enhance cost-effectiveness, easiness-of-use in combination with selectivity and sensitivity in virus detection during severe pandemic conditions, and a more effective variant tracking by optimizing the access to sequencing resources even during the acute phases of pandemic.

1. Introduction

On May 5th, 2023 the World Health Organization officially declared the end of the COVID-19 pandemic. With more than 7 million deaths worldwide (up to December 2024[1]) and incalculable socio-economic consequences, this event unrevealed all limits of medical programs and available technologies for emergency management, and the importance of investments in biology and bioengineering for the development of therapeutics and diagnostics approaches beyond the current state-of-the-art.

The management of the COVID-19 pandemic relied on the early detection of the virus in biological samples (mostly nasopharyngeal swab and saliva), and on the capability of tracking the diffusion of variants to adapt therapies and diagnostic tools to the evolution of the virus. The detection involved mainly two different approaches: immunosensing by lateral-flow tests, based on capturing the SARS-CoV-2 by anchoring its spike proteins with specific antibodies, and genetic detection of viral RNA. The first approach ensures the lower cost for users and the lower time-to-result, but their effectiveness in detection is maximum after symptoms appear. Moreover, since specificity is strongly reliant on immunological detection of the spike protein, even small changes in its structure can strongly affect the specificity and accuracy of the test, thus resulting in higher probability of false negatives. Molecular detection ensures the best performance in terms of early sensitivity and specificity, but the need of virus processing to extract its RNA and, above all, its amplification by Polymerase Chain Reaction (PCR) significantly increases the time-to-result.[2]

Virus variant tracking is a fundamental activity for a proper management of the pandemic, since the effects of new variants can significantly impact on public health systems. At the

S. Lai
Department of Electrical and Electronic Engineering
University of Cagliari
Piazza d'Armi, Cagliari 09123, Italy
E-mail: stefano.lai@unica.it

The ORCID identification number(s) for the author(s) of this article can be found under https://doi.org/10.1002/adsr.70000

DOI: 10.1002/adsr.70000

R. Cusano, G. Fotia
CRS4: Centro di Ricerca
Sviluppo e Studi Superiori in Sardegna
Loc. Piscina Manna, Edificio 1, Pula 09050, Italy

A. Scano
Department of Surgical Sciences
University of Cagliari, Cittadella Universitaria di Monserrato
S.P. 8 km 0,700, Monserrato 09042, Italy

A. Scano
University Hospital of Cagliari – AOU
Cittadella Universitaria di Monserrato
S.P. 8 km 0,700, Monserrato 09042, Italy

A. Bonfiglio
University School for Advanced Studies (IUSS)
Piazza della Vittoria 15, Pavia 27100, Italy

state-of-the-art, new variants discovery and tracking are mainly based on Sanger sequencing or Next Generation Sequencing (NGS) technologies of viral RNA extracted from saliva and nasopharyngeal swab samples, subsequently aligned *in silico* with respect to those previously known sequences. Moreover, since an amplification of viral RNA is fundamental to ensure a correct sequencing, laboratories have to share the PCR resources to virus detection and tracking: during COVID-19 pandemic this actually resulted in a limited tracking, since diagnosis was often considered more important in the low-term socio-economical management of impacts.[3]

The significant probability of a next pandemic within this century[4] induces the scientific community to thoroughly consider the COVID-19 experience and produce innovative approaches for reducing social, medical and economic impacts. As regards diagnosis, this involves novel technologies that can combine the low costs and fast results of immunological testing with the high accuracy and sensitivity of RNA detection since the very early stages of the infection (i.e., even before symptoms appears),[5] and this mostly implies the avoidance of the PCR amplification. In terms of tracking, since sequencing is unavoidable to derive the correct sequence of new variants, the development of easier and faster approaches that can be used for sample screening would be of great benefit.

In order to fulfill these goals, the scientific community has considered biosensors as a valuable solution since the very beginning of COVID-19 pandemic. Biosensors integrates biochemical detection and signal transduction in many forms, potentially allowing the development of compact, cost-effective and user-friendly instrumentation for biomolecular detection in different application scenarios.[6,7] PCR-free virus detection has been demonstrated in electrochemical[8–12] and electronic biosensors: in particular, the latest technology results attractive for its high potential of miniaturization, cost-effective fabrication and intrinsic signal amplification.[13] To date, graphene-based field-effect transistors (GFETs) have been demonstrated suitable for PCR-free viral RNA sensing,[14–17] but only in a few examples based on low-scale fabrication approaches, which doesn't perfectly fulfill the requirements of a low-cost technology suitable for disposable sensing platforms. In this sense, organic flexible electronics is a valuable approach for the fabrication of FET-based biosensors, namely bioFET, by means of cost-effective, large-area production processes:[18] nonetheless, this technology has been mostly explored for the immunological detection of SARS-CoV-2,[19–21] and to date there aren't example in literature of PCR-free molecular detection and approaches for variant tracking.

In this paper, we report the employment of a bioFET structure, namely Organic Charge-Modulated FET (OCMFET) for the PCR-free detection of viral RNA, and the recognition of variants on PCR-amplified amplicons based on sensor selectivity to polymorphisms, without the need for sequencing. The OCMFET working principle has been thoroughly explored for the recognition of DNA hybridization,[22–25] resulting in world-record sensitivity and selectivity performance among organic semiconductor-based biosensors.[23] Recently, its employment for the PCR-free epigenetic biomarker detection in genomic samples has been reported for the screening of colorectal cancer.[25] In the experiments in this paper, SARS-CoV-2 and its variants were employed as a significant benchmark to demonstrate the potential feasibility of the proposed approach at a proof-of-concept level. Thanks to the employment of Peptide Nucleic Acid (PNA) probes, viral RNA fragments in the range of the femtomolar has been detected. Moreover, thanks to the robustness of the OCMFET approach, the selectivity to single nucleotide variants was enhanced by the use of PNA probes compared to those based on standard nucleic acids. In experiments performed with amplicons obtained from two different regions of the ORF1 frame of the viral genome, SARS-CoV-2 sequences were successfully distinguished from specific variants of SARS-CoV-2 VOC-202012/01 (Alpha variant). In both cases, RNA detection occurs in 20–40 min, resulting faster than common molecular approaches and comparable with immunologic detection. Therefore, this approach fulfills two different roles: the highly sensitive, PCR-free molecular detection of virus with a cost-effective technology, competitively priced with immunologic sensing, and the recognition of the specific variant through sample amplification but without the need for sequencing. Although preliminary and requiring further investigations, the proposed results potentially pave the way for the application of the proposed approach in next-generation low-cost, rapid screening tool for virus mutation tracking.

2. Results and Discussion

2.1. Proof-Of-Concept Evaluation of Detection Strategy

Figure 1a shows the working principle of OCMFET-based viral RNA detection. As thoroughly discussed elsewhere,[26] the OCMFET is a floating gate transistor-based charge sensor, capable of charge variations transduction in a close proximity of a part of the floating gate directly exposed to the environment (from now on, the sensing area) into a variation of the threshold voltage. Indeed, the charge on the sensing area influences charge distribution inside the floating gate, involving the amount of charge available in the transistor structure for inducing channel formation at the semiconductor-insulator interface. Charge carrier variation in the sensing area, ΔQ, and the corresponding threshold voltage variation, ΔV_{TH}, are linked by the total capacitance in the layout, C_{SUM}, through the Equation (1)

$$\Delta V_{TH} = -\frac{\Delta Q}{C_{SUM}} \tag{1}$$

Since threshold voltage varies, the transistor output current varies accordingly. The latest equation also relates the device performances and the layout geometrical features through the C_{SUM}, thus making possible a precise tailoring of sensing capability by means of defined design rules.[23] The specificity of the sensor depends on the functionalization of the sensing areas by means of receptors specific to the investigated analytes. For viral RNA detection, the complementary binding between the target sequence and the receptor layer (from now on, the probe layer) is employed to anchor the viral RNA to the sensing surface. Since RNA is a negatively-charged molecule, a shift in threshold voltage occurs, and consequently a variation of the output current.

In this application, PNA probes, in which the phosphate deoxyribose backbone has been replaced by uncharged linkages, were chosen for their higher double helix binding stability with

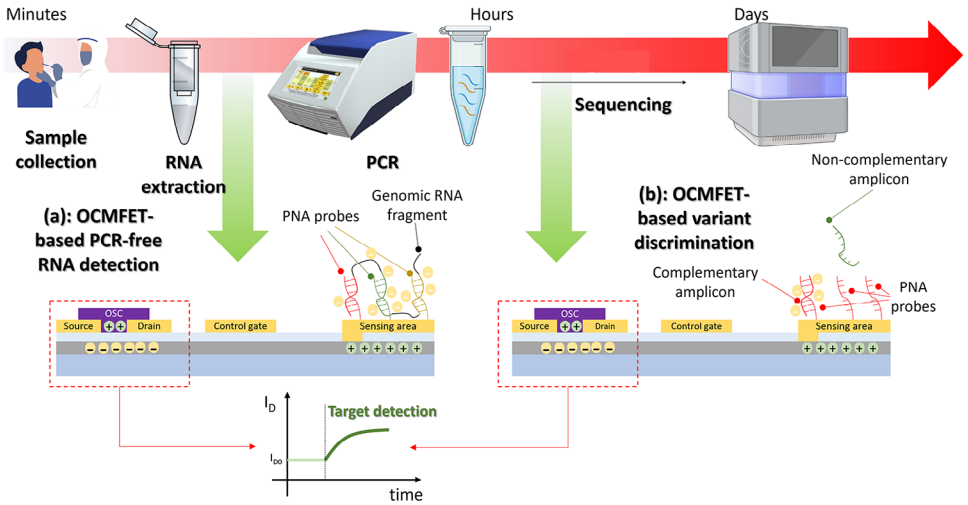

Figure 1. OCMFET-based virus detection and variant tracking versus state-of-the-art procedures: a) OCMFET-based PCR-free genomic viral RNA detection by means of PNA probes capable of RNA fragment capture of the sensing surface; b) amplicons detection for variant recognition as screening approach supporting the selection of samples for RNA sequencing: specific PNA probes recognize RNA sequences of a defined version of the virus. The negative charge of captured targets modulates charge distribution in the transistor, determining an output current variation proportional to target concentration.

RNA compared to DNA-RNA hybrid and for their resistance to nucleases and proteases. Moreover, PNAs guarantee higher specificity compared to DNA or RNA probes, since the presence of a single non-pairing makes the hybrid double helix much less stable than a double helix of RNA-RNA, DNA-DNA or RNA-DNA.[27] Preliminary characterization of PNA probes performance over DNA counterparts was evaluated by means of optical analysis on fluorescent-labelled targets: results are described in Supporting Information (Figure S2, Supporting Information and related text).

Three PNA sequences, namely P1, P2 and P3 were synthetized to be complementary to a 150 bp sequence in the ORF3a region of viral RNA, which resulted specific for SARS-CoV-2 virus compared to other coronavirus. The three probes have been designed (details in the Experimental section) to bind this area in three different points, thus improving the capture efficiency of a long RNA oligonucleotide. Sequences of the probes are reported in **Table 1**.

Preliminary tests were carried out to verify the effectiveness of functionalization procedure, and the correct functionality of sensors in detecting long RNA fragments. To this aim, probes provided with cyanine-3 (Cy3) fluorescent dyes were purchased, allowing an optical validation of the functionalization protocol (Figure S3, Supporting Information). The detection validation was performed using a synthetic RNA (sRNA) target of 120 bp length, which is the maximum length that the manufacturer could guarantee with a high degree of purity. Results of target detection are reported in **Figure 2**, in terms of percentage current variation in real time (a) and average among three independent experiments (b). Percentage current variation is $100 \cdot \Delta I_D / I_{D0}$, being $\Delta I_D = I_D - I_{D0}$, and specifically I_D the output current of the transistor, while I_{D0} is its stable value before the addition of the target molecule. A stabilization stage is performed to ensure that any residual drift in I_{D0} is negligible in a relevant timespan (Figure S4, Supporting Information). A solution containing the RNA target with a final concentration of 1 μM was spotted on the sensing area of the device at t = 0. More details about the measurement conditions are available in the Experimental section. Since each sensor hosts three different OCMFET, validation tests were possible: in particular, for each device,

Table 1. Molecules for viral RNA detection tests.

Molecule name	Type	Sequence (5′-3′)	BP Content
P1	Probe	[Thiol]-GTTCAGAAATAGGACTTGTTGTGCCATCACCG	32
P2	Probe	[Thiol]-CAGTCTTTTATCACTTAGCCATTTTTTCAG	30
P3	Probe	[Thiol]- ACTATTGTAAGGTATACAATAGTCGTAAC	29
sRNA	Target	ATAGTGTAACTTCTTCAATTGTCATTACTTCAGGTGATGGCACAACA AGTCCTATTTCTGAACATGACTACCAGATTGGTGGTTATACTGAAAAATGGG AATCTGGAGTAAAAGACTGTG	120
gRNA	Target	CTAATTGTTACGACTATTGTATACCTTACAATAGTGTAACTTCTTCAATTGTCAT TACTTCAGGTGATGGCACAACAAGTCCTATTTCTGAACATGACTACCAGATTG GTGGTTATACTGAAAAATGGGAATCTGGAGTAAAAGACTGTG	150

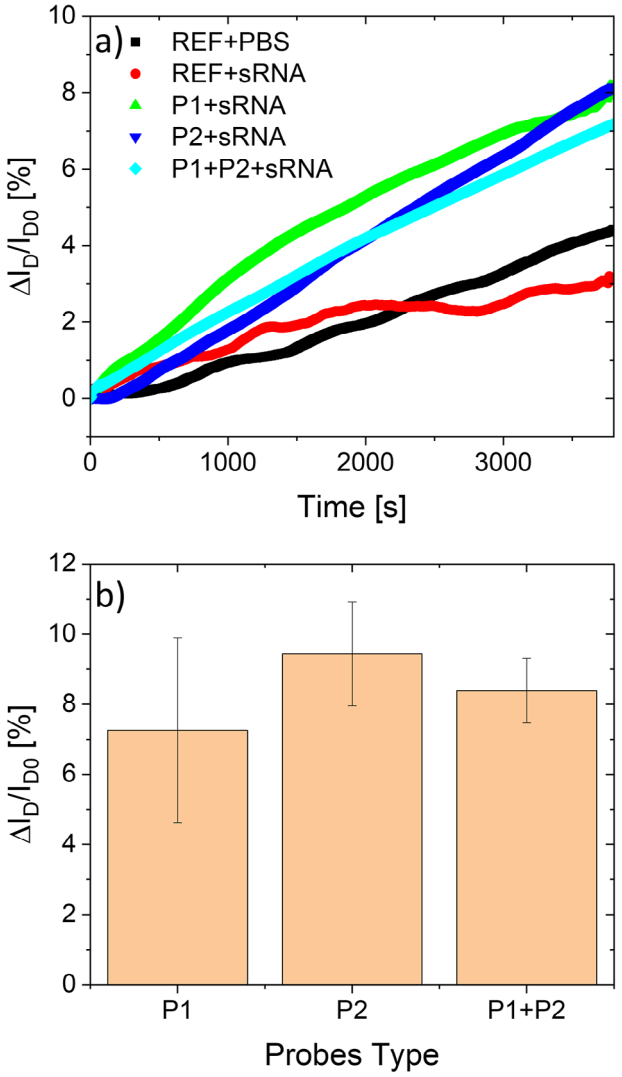

Figure 2. Preliminary characterization of OCMFET-based RNA sensors with synthetic target: a) representative percentage current variation in time for blank reference exposed to PBS (black), blank reference exposed to the target molecule (red) and functionalized sensors exposed to the target molecule at a concentration of 1 μM with different probe layer configurations (single probe P1– green– and P2– blue– and combined probe layer P1+P2– cyan). b) Average current variation for different probe layer configurations evaluated in three different experiments.

two OCMFETs were not functionalized (reference devices, REF), while the third was functionalized with a single probe (P1 and P2) or with a combination of probes (P1+P2). In these experiments, only P1 and P2 probes were considered, since P3 sequence was designed to bind a 150 bp target in the 5′ end, thus being substantially not usable in the 120bp-long synthetic target. As shown in Figure 2a, REF devices shown an increase of the current with similar dynamics when exposed to pure PBS and to the target sequence (concentration 1 μM): this current variation represents an intrinsic drift of sensor, probably related to a residual bias-stress, that is, a continuous trapping of charge carriers at the semiconductor-insulator interface. These experiments allow defining a noise margin for the evaluation of the specific response of the sensor. As a matter of fact, when functionalized devices are exposed to the complementary target sequence, a much larger response was noticed, with a clearly distinguishable dynamic with respect to the drift. This was obtained in both single-probe functionalized devices and with P1+P2 probe layer. In repeated experiments (Figure 2b), the three different configurations tested don't significantly vary, although P2 results slightly more efficient in terms of signal amplitude and reproducibility, and P1+P2 have similar performances. This can be coherent with the position of the anchoring point of P2 in the target sequence, that is, near the 3′ end and thus neared to the sensing surface, while P1 is complementary to a portion of the molecule neared to the 5′ end: when P1 probes are used alone, the hybridization efficiency is probably lower due to the encumbrance of the remaining part of the target. Nonetheless, in all configurations adopted, the functionality of the sensor was fully demonstrated.

2.2. OCMFET as PCR-Free Viral RNA Detection

After these preliminary tests, genomic RNA detection was considered. Genomic RNA coming from standard positive for throat swab validation and from negative patients were fragmented into 150 bp genomic RNA targets (gRNA), prepared as described in the Experimental Section; hybridization tests were carried out following the same procedure of previously reported tests. **Figure 3** reports examples of real-time current variation (a) and average results over three independent repetitions of the test (b). Negative samples were used as reference to define the tolerance band of sensor response: also in this case, an aspecific drift was recorded, not exceeding (in average) the 1.5% of current variation during the experiment. Different concentrations of positive samples were tested, ranging from 10^2 to 10^5 molecules per microliter, that is, typical values from a low positive to a fully positive response. It is possible to observe that for lower concentrations (10^2-10^3 molecules per microliter, equivalent to 10^{-17}-10^{-16} M), the sensor response can't be clearly discriminated from the negative control, while for larger concentrations (10^4-10^5, that is, 10^{-15}-10^{-14} M) the sensor response is clearly beyond the negative control, being averagely two-four times larger. Static characteristic curve acquisition allowed verifying that the current variation was actually related to a threshold voltage shift, following OCMFET working principle (Figure S5, Supporting Information). Although preliminary, these results clearly show the potentialities of the OCMFET as genomic RNA sensor, which is detected at valuable conditions without the need for PCR amplification and with minimum sample preparation. It is noteworthy that device performances in terms of sensitivity are several order of magnitude larger than the one previously obtained in DNA hybridization detection by OCMFET (1 pM of measured concentration, extrapolated limit of detection of 100 fM[23]): this improved sensitivity can be related to the employment of PNA probes, which allow avoiding the charge repulsion between probes and targets and thus making hybridization more efficient also at lower concentrations. Moreover, these performances can be further improved starting from these preliminary results, taking advantage of the design rules of the OCMFET, allowing foreseeing even lower detection limits by optimizing the layout to the requested

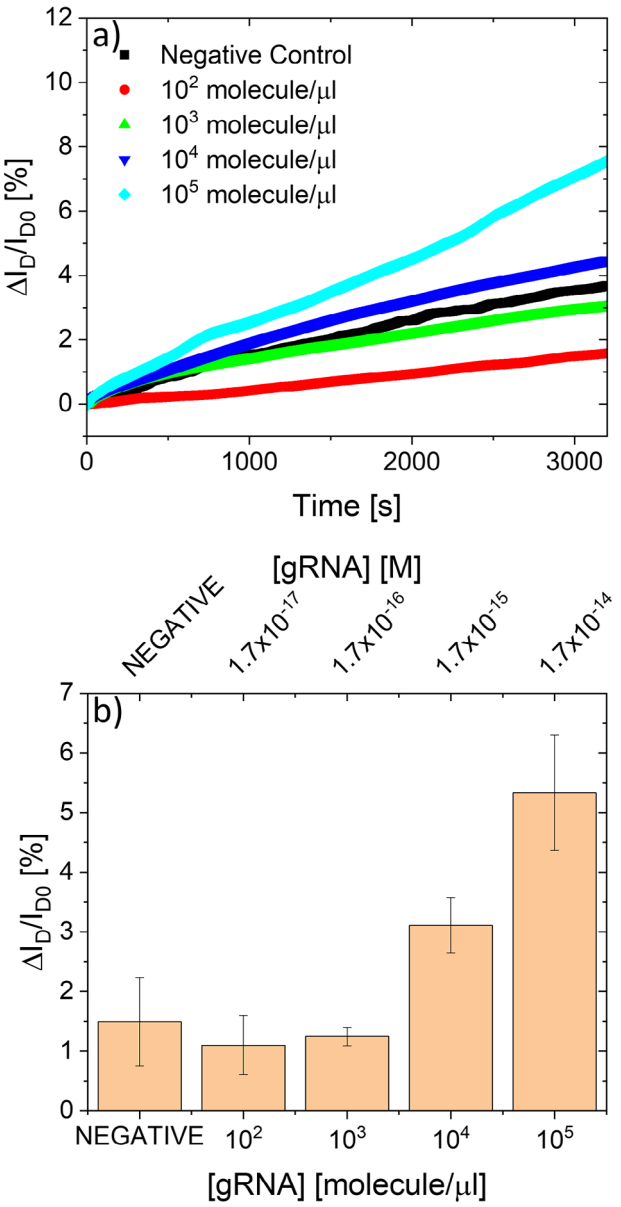

Figure 3. OCMFET-based, PCR-free genomic viral RNA detection. a) Representative percentage current variation in time for functionalized devices exposed to a negative control (black) and increasing target concentration, expressed in molecules·µl^{-1}, of 10^2 (red), 10^3 (green), 10^4 (blue) and 10^5 (cyan). b) Average percentage current variation obtained in three different and independent experiments for each concentration; the top x-axis reports the corresponding target molar concentration.

concentrations.[23] For instance, reducing the total area of the floating gate (and thus the area of the control capacitor), together with increasing the sensing area/floating gate area ratio, would bring to higher sensitivity performances.

Table 2 compares performance of the proposed sensor with respect to other field-effect based sensors.[14–17] The minimum tested concentrations (limit of quantification) are indeed comparable with most of the state-of-the-art, as well as time-to-result. It is noteworthy that the reference results are obtained on solid supports (glass or Silicon) with graphene prepared in suspensions and subsequently collected on supports. In contrast, the performances here reported are obtained in technological processes common to flexible organic electronics, which are more suitable for scaling up to cost-effective, large-area mass production processes. These results are therefore relevant for the future development of affordable, mass-screening kits. Moreover, the previously-discussed optimization steps in terms of layout dimensions would potentially further improve the sensing ability of devices, thus making them even more competitive in terms of sensitivity.

Table 2. Comparison of proposed approach with relevant literature.

Reference	Limit of Quantification	Time	Substrate
[14]	1 fM	2 min	Silicon
[15]	0.1 fM	2 min	Silicon
[16]	0.003 copies µl^{-1}	15 min	Silicon
[17]	1 aM	30 min	Glass
[this paper]	1.7 fM	50 min	PET

2.3. OCMFET for Variant Discrimination

The mechanism of viral RNA detection by OCMFET can be adapted to the discrimination of variants without the need for sequencing the whole viral genome. This approach, described in Figure 1b, relies on the robustness of the OCMFET detection to polymorphisms, thoroughly demonstrated in DNA/DNA systems:[22,23] if amplicons are generated by PCR, OCMFET devices provided with specific probes are potentially capable to discriminate among different viral sequences with a limited number of mutations. Therefore, this strategy can be used to perform a sample screening to optimize mutation sequencing: not only a reduced number of samples (i.e., those selected as possible mutating viruses by OCMFET screening) will be sequenced, but their selection (at the state-of-the-art, purely statistical) will be guided by robust measurement data.

To demonstrate this further functionality, two similar SARS-CoV-2 viruses, that is, the original Wuhan-Hu-1 and its SARS-CoV-2 VOC-202012/01 (Alpha) variant were considered. The latest differs from the original virus from some deletion in the ORF3a region of the spike protein (see details in the Experimental section): amplicons have been designed as 73 and 86 bp oligonucleotides including the areas with strong mutations. In particular, a first kind of amplicons was designed in a region containing a 6 bp deletion (from now on, Del69) in the Alpha variant with respect to the Wuhan, thus resulting in a polymorphic content of ≈ 8%, while a second amplicon includes a maximum of 3 bp deletion (Del114, 3.7% polymorphic content). In this way, four amplicons are defined: two for original Wuhan virus (A_Wuhan1 and A_Wuhan2) and two for the Alpha variant (A_alpha1 and A_alpha2). PNA probes were designed to be complementary to each of this target: all sequences are reported in **Table 3**.

Figure 4 reports representative real-time measurement for amplicon detection (a,b) and average percentage current varia-

Table 3. Probes and Amplicons used for variant detection tests.

Molecule name	Type	Sequence (5′-3′)	BP content
P_Wuhan1	Probe	[Thiol]-AACCTCTTAGTACCATTGGTCCCAGAGACATGTATAGC ATGGAACCAAGTAACATTGGAAAAGAAAGGTAAGA	73
P_Wuhan2	Probe	[Thiol]-GAACTCACTTTCCATCCAAGTTTTGTTGTTTTTGTGGTAA TAAACACCCAAAAATGGATCATTACAAAATTGAAATTCACAGACTT	86
P_Alpha1	Probe	[Thiol]-AACCTCTTAGACCATTGGTCCCAGAGATAGCA TGGAACCAAGTAACATTGGAAAAGAAAGGTAAGA	67
P_Alpha2	Probe	[Thiol]-GAACTCACTTTCCATCCAACTTTTGTTGTTTTTGTGG TAAACACCCAAAAATGGATCATTACAAAATTGAAATTCACAGACTT	83
A_Wuhan1	Amplicon	TCTTACCTTTCTTTTCCAATGTTACTTGGTTCCATGC TATACATGTCTCTGGGACCAATGGTACTAAGAGGTT	73
A_Wuhan2	Amplicon	AAGTCTGTGAATTTCAATTTTGTAATGATCCATTTTTGGGTGT TTATTACCACAAAAACAACAAAAGTTGGATGGAAAGTGAGTTC	86
A_Alpha1	Amplicon	TCTTACCTTTCTTTTCCAATGTTACTTGGTTCCA TGCTATATCTGGGACCAATGGTACTAAGAGGTT	67
A_Alpha2	Amplicon	AAGTCTGTGAATTTCAATTTTGTAATGATCCATTTTTGGG TGTTTACCACAAAAACAACAAAAGTTGGATGGAAAGTGAGTTC	83

tion over three independent experiments (c). Each experiment used an OCMFET platform functionalized with a single probe (P_Wuhan1 or P_Wuhan2), with one device exposed to a negative control, a device exposed to the complementary amplicon and the last exposed to its mutated counterpart. If the device is functionalized with the probes P_Wuhan1 for the discrimination of Del69 (Figure 4a), it is possible to observe that a positive response is only obtained for the complementary amplicon A_Wuhan1, while A_alpha1 results in an almost absent response, comparable with the negative control. Also for Del114 (Figure 4b), P_Wuhan2 results more effective in detecting A_Wuhan2 than A_alpha2 (which has a response not distinguishable from negative control), but in this case a lower noise margin is generally obtained. This can be related to the lower polymorphic character of mutated sequence with respect to the Wuhan original sequence, while the lower extent of the response with respect to the previous experiment has been ascribed to a lower viral content in the sample used for template extraction, as also verified by TaqMan probes analysis on PCR outcomes. Average results (Figure 4c) confirm that the correct discrimination of mutations is well reproducible over independent experiments, showing that the multi-sensor platform allows a clear identification of possible virus variants to be further explored by sequencing. As further confirmation on the obtained results, the same experiments have been carried out using probes complementary to the mutated sequences (P_Alpha1 for Del69 and P_Alpha2 for Del114): results, reported in Figure S6 (Supporting Information), are substantially the same of previous experiment, even if the amplitude of the response is slightly lower, possibly due to lower thermodynamic properties of mutated probes due to self-hybridizing areas of the sequence.

3. Conclusion

In this paper, electronic detection of viral RNA by means of an organic electronic-based sensors has been discussed. The proposed strategy is suitable for the recognition of genomic RNA extracted from human samples without the need for PCR amplification, integrating the user-friendly and fast analysis of antigenic tests with the selectivity and sensitivity of molecular recognition. The combination of an highly-sensitive and selective DNA hybridization sensor with PNA probes allows demonstrating genomic RNA detection in the femtomolar range, being comparable with typical viral strength of early-detected positive by PCR-based approaches. The same approach resulted effective in discriminating variants by the robustness of the sensor-PNA system to polymorphism. Two different SARS-CoV-2 sequences, with a limited polymorphic content, were successfully recognized, thus showing the potentiality of the proposed approach in acting as screening procedure to select samples to be further explored for a complete sequencing for effective variant tracking. It is worth noting that the proposed results demonstrates the functionality of the proposed approach at a proof-of-concept level. However, a more in-depth analysis of sensor performance, including statistically significant sample sizes and control experiments, is necessary to fully characterize the device's features. Despite these current limitations, the innovative application of electronic biosensing in virus detection and tracking here reported could inspire new strategies for a more effective and straightforward management of pandemic and epidemic crisis, optimizing cost-effectiveness and simplicity of sample preparation and handling with rapid, selective and early detection and variant tracking.

4. Experimental Section

Device Fabrication: OCMFET-based sensing platforms have been fabricated on 175 µm-thick polyethylene terephthalate (PET, Goodfellow) substrates in a bottom-gate, bottom-contact structure. Each platform hosts three independent OCMFET, used for differential tests. Substrates have been cleaned with acetone, isopropyl alcohol and deionized water, before the deposition of a 100 nm thick layer of aluminum by thermal evaporation at a pressure of 10^{-5} Torr. The structure of floating gates was first defined by a standard photolithographic process, and then cured at 50 °C for 12 h to obtain a surface layer of aluminum oxide. Then, chemical

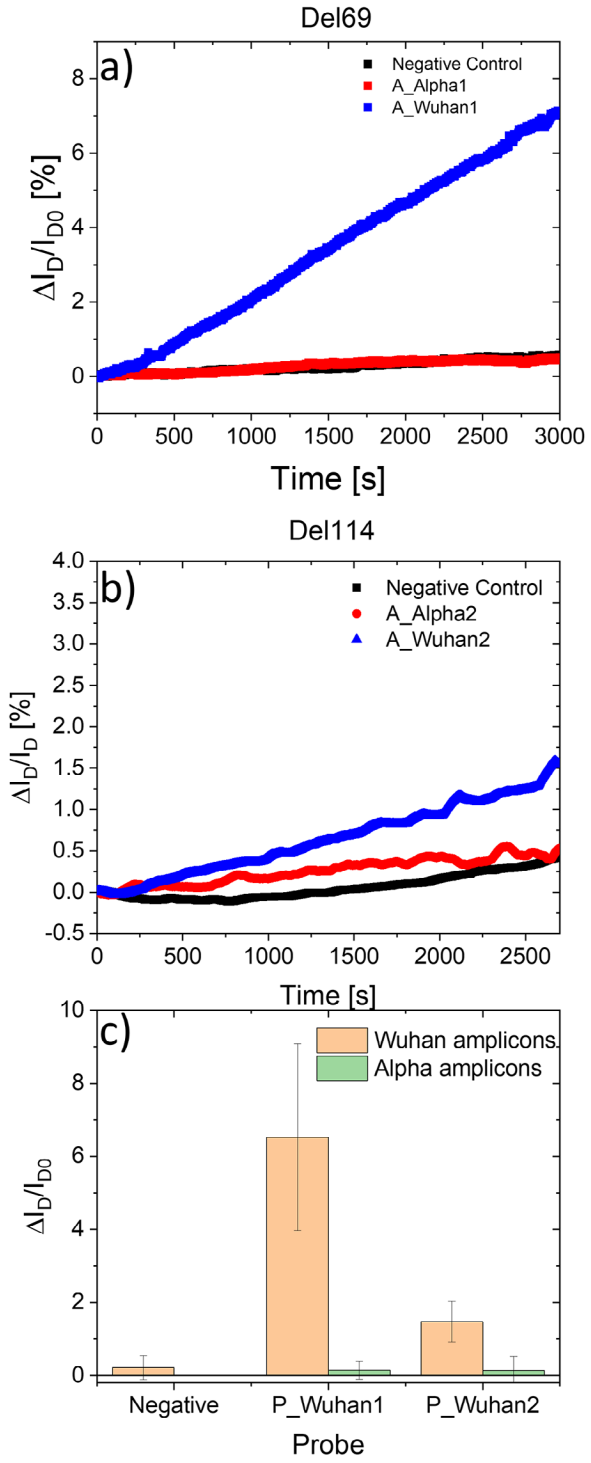

Figure 4. OCMFET-based variant discrimination: a) Representative percentage current variation in time for a device functionalized with probe P_Wuhan1 exposed to negative control (black), mutated amplicon A_Alpha1 with deletion Del69 (red) and complementary amplicon A_Wuhan1 (blue). b) Representative percentage current variation in time for a device functionalized with probe P_Wuhan2 exposed to negative control (black), mutated amplicon A_Alpha2 with deletion Del114 (red) and complementary amplicon A_Wuhan2 (blue). c) Average current variation obtained in three independent experiments for each probe-amplicon configuration.

vapor deposition of a 170nm-thick Parylene C (Specialty Coating Systems) layer was performed: the hybrid aluminum-Parylene C dielectric has a capacitance per unit area of 15 nFcm^{-2}, which ensures the low voltage operation of the device. The transistor structures, the control capacitors and the sensing areas are fabricated by thermal evaporation of gold (pressure 10^{-5} Torr) and photolithographic patterning: in particular, a self-alignment process was employed for reducing source/drain overlaps with the floating gate for an improved OCMFET sensitivity.[28] Geometrical features of the final layout are reported in Table S2 (Supporting Information). The transistors were completed with the drop casting of a 1 wt.% solution of 6,13-Bis(triisopropylsilylethynyl)pentacene ≥99% (TIPS pentacene, Sigma Aldrich) in anisole anhydrous (Sigma Aldrich), let dry at room temperature and ambient conditions. Custom 3D-printed (using a Makerbot Replicator 2x, Makerbot), acrilonitrile butadiene styrene (ABS, Innofil) fluid chambers were glued on the sensing areas using a poly(dimethylsiloxane) (PDMS, Sylgard 186, Dow Corning)-based glue. The top part of fluid chambers was capped with a film of transparent PDMS (Sylgard 184, Dow Corning). To improve shelf-life and enhance the stability of electrical performance throughout experiments, devices were encapsulated with a 2 µm-thick Parylene C layer: the encapsulation of sensing areas was prevented by the fluid chambers, thus ensuring a free gold surface for device functionalization. A rule-of-thumb evaluation of the cost of the fabrication process at a semi-industrial scale of the proposed technology, detailed in Supplementary Information, is of about 0.04 Euro cm^{-2}, with a cost for a single device in the range of 0.81 Euros (see Supporting Information for a detailed analysis of production costs).

Probes design for SARS-CoV-2 RNA genomic detection: A 120 nucleotides target region, corresponding to the portion from 25 860 to 26 009 nt in the viral ORF3a gene of the SARS-CoV-2 Wuhan-Hu-1 reference genome (GenBank ID NC_045512.2), was selected using BLAST search versus nucleotide and Betacoronavirus databases on the basis of the least homology with other sequences. Three different areas of this sequence with different thermodynamic properties were selected varying their GC content to design complementary probes for target capture (P1, P2 and P3). PNA probes complementary to these regions, and a synthetic 120 bp RNA sequence, where purchased by Panagene.

Amplicons and Probes Design for Variant Tracking: The DNA oligos used in this study were designed using the wild-type isolate Wuhan-Hu-1, GenBank accession number NC_045512.2, and the sequence of the clinical isolate Cagliari335, alpha variant, GISAID ID EPI_ISL_2885744. The previously mentioned reference sequence Cagliari335 was obtained from nasal swabs that had previously tested positive for SARS-CoV-2 by using the Genesis PCR real-time kit (Primerdesign Ltd., UK, threshold cycle of 15.00). For NGS sequencing, the SuperScript VILO cDNA synthesis kit (Invitrogen, Carlsbad, CA, USA) was used to create cDNA using 10 µl of RNA extract, following the manufacturer's instructions. The NGS procedure was performed by using Ion Torrent NGS Instrument with Ion torrent AmpliSeq panel sequencing (Thermo Fisher Scientific, USA).

Two regions of the spike protein gene sequence were considered in the Wuhan-Hu-1 and Cagliari335 sequences, characterized by the maximum number of mismatched bases: a first region consisting of 73 bp, in which the alpha variant shows a 6 bp deletion (from now on, Del69), and a second one of 86 with a 3 bp deletion in the alpha variant (from now on, Del114). Amplicons for Wuhan-Hu-1 and Cagliari335 in the two regions (A_Wuhan1 and A_Wuhan2, and A_alpha1 and A_alpha2, for Del69 and Del114 respectively) were obtained by PCR reaction, carried out using Taq-PathTM 1-Step RRT-PCR MasterMix (Life Technologies, Corp in Carlsbad, Carlsbad, CA, USA) and considering the manufacture instructions. Additionally, heat-labile uracil–DNA–glycosylase (UDG, Roche Molecular Biochemicals) and 2 L of RNA extract was used. The PCR profile, conducted by using a CFX 96 apparatus (Bio-Rad laboratories USA), was as follows: i) an initial uracil–DNA–glycosylase (UNG) incubation at 25 °C for 2 min, ii) RT incubation at 50 °C for 15 min and iii) 40 cycles of 3 s at 95 °C, 30 s at 60 °C. The PCR amplicon (about in mean 158 bp) was used as target for electrochemical experiments. To ensure the absence of potential secondary PCR products, PCR products were analyzed by 0.8% agarose gel electrophoresis.

Four PNA probe sequences were thus designed (and purchased by Panagene) for binding the above mentioned amplicons: P_Wuhan1 and P_Wuhan2 for the amplicons obtained from Wuhan-Hu-1, and P_alpha1 and P_alpha2 for the amplicons of mutated virus with deletion Del49 and Del114 respectively.

Sensor Functionalization: The functionalization of sensing areas with PNA probes was carried out exposing the gold surface to a solution 25 mM of phosphate buffer solution (PBS), 25 mM of sodium chloride (NaCl), containing PNA probes at a concentration of 10 μM and 1-mercapto-6-hexanol (MCH, Sigma Aldrich) at a concentration of 1 μM. For genomic RNA detection, a mix of PNA probes P1, P2 and P3 (with a total concentration of 10 μM) was used; for amplicons detection, a single probe was used. MCH molecules are well known co-molecules used to optimize the steric hinderance and probe film morphology of effective target capture. To ensure the chemical bond formation and probes re-ordering on surfaces, the sensing areas were exposed to the functionalization solution for at least 12 h, then rinsed with pure PBS to remove the a-specifically adsorbed molecules.

Preparation of Genomic RNA Fragments: Three different samples were considered for genomic RNA detection experiments. A positive control for throat swab, containing complete viral RNA of SARS-CoV-2 Wuhan virus, was used as template for the preparation of solutions at different molecule density (from 10^5 to 10^2 molecules per microliter). A negative control, that is, a purified extract from throat swab of a negative patient, was also used. Both samples were sonicated in cold water using glass beads for 70 min, alternating 30 s of active sonication to 30 s resting time, to obtain 150 bp RNA fragments, following an available protocol.[29]

Electrical Characterization: Device performances were initially evaluated by measuring transistor characteristics curves and extrapolating figures of merits such as threshold voltage and charge carrier mobility. Measurements have been carried out by means of a Keithley SourceMeter 2636, controlled by a custom Matlab software. Hybridization detection measurements have been carried out in ambient conditions using the same instrumentation, by measuring the drain current in real time at fixed drain-to-source voltage ($V_{DS} = -5$ V) and with a square-wave variable gate-to-source voltage, used to minimize the bias stress.[30] The gate voltage values were adapted to bias different devices at same overthreshold conditions: typical settings were $V_{GS,ON}$ =-3 V, $V_{GS,OFF}$, 0, frequency 2.5 Hz, duty cycle 30%.

Ethical Statement: All human samples originate from the screening procedures of COVID-19 pandemics carried out at the "Azienda Ospedaliera Universitaria" of the University of Cagliari; as teaching hospital, all the consent forms signed at the screening include the possibility to using clinical, biochemical, and imaging data even for research purposes. In this perspective, a formal ethical approval by the Independent Review Board was not required in accordance with the policy of the Institution for non-interventional (observational) retrospective studies concerning clinical/biochemical/imaging. Moreover, samples used as target sequences, or template for amplicons production, were anonymized. Therefore, the procedures for sample collection and management comply with the principles of the Declaration of Helsinki.

Supporting Information

Supporting Information is available from the Wiley Online Library or from the author.

Acknowledgements

S.L., R. C. and G. F. gratefully acknowledge Sardegna Ricerche for partially funding the activities under the project "RNA4CoV" (Messa a punto di un sensore portatile per uno screening preliminare del SARS-CoV-2), under the program "SR4COVID" (det. dg 543 pst, 28/04/2020).

Conflict of Interest

The authors declare no conflict of interest.

Data Availability Statement

The data that support the findings of this study are available from the corresponding author upon reasonable request.

Keywords

direct detection, organic biosensors, PCR-free, SARS-CoV-2, variant monitoring

Received: December 20, 2024
Revised: March 28, 2025
Published online: May 8, 2025

[1] World Health Organization, Cumulative number of COVID-19-related deaths worldwide, https://data.who.int/dashboards/covid19/deaths, (accessed: December, **2024**).
[2] T. R. Mercer, M. Salit, *Nat. Rev. Genet.* **2021**, *22*, 415.
[3] O. Vandenberg, D. Martiny, O. Rochas, A. van Belkum, Z. Kozlakidis, *Nat. Rev. Microbiol.* **2021**, *19*, 171.
[4] M. Marani, G. G. Katul, W. K. Pan, A. J. Parolari, *Proc. Nat. Acad. Sci.* **2021**, *118*, e2105482118.
[5] S. K. Patel, J. Surve, J. Parmar, K. Ahmed, F. M. Bui, F. A. Al-Zahrani, *IEEE Rev. Biomed. Eng.* **2023**, *16*, 22.
[6] R. Liu, L. He, Y. Hu, Z. Luo, J. Zhang, *Chem. Sci.* **2020**, *11*, 12157.
[7] W. Zhang, Y. He, Z. Feng, J. Zhang, *Microchim. Acta* **2022**, *189*, 128.
[8] S. M. El-Sheikh, D. I. Osman, O. I. Ali, W. G. Shousha, M. A. Shoeib, S. M. Shawky, S. M. Sheta, *Appl. Surf. Sci.* **2021**, *562*,150202.
[9] C. Pina-Coronado, Á. Martínez-Sobrino, L. Gutiérrez-Gálvez, R. Del Caño, E. Martínez-Periñán, D. García-Nieto, M. Rodríguez-Peña, M. Luna, P. Milán-Rois, M. Castellanos, M. Abreu, R. Cantón, J. C. Galán, T. Pineda, F. Pariente, Á. Somoza, T. García-Mendiola, R. Miranda, E. Lorenzo, *Sens. Actuat. B-Chem.* **2022**, *369*,132217.
[10] W. Heo, K. Lee, S. Park, K.-A. Hyun, H.-I. Jung, *Biosens. Bioelectron.* **2022**, *201*, 113960.
[11] L. Kashefi-Kheyrabadi, H. Vu Nguyen, A. Go, C. Baek, N. Jang, J. M. Lee, N.-H. Cho, J. Min, M.-H. Lee, *Biosens. Bioelectron.* **2022**, *195*, 113649.
[12] N. Syafirah Zambry, M. S. Awang, K. K. Beh, H. H. Hamzah, Y. Bustami, G. A. Obande, M. F. Khalid, M. Ozsoz, A. A. Manaf, I. Aziah, *Lab Chip* **2023**, *23*, 1622.
[13] H. Yu, H. Zhang, Z. Liu, L. Feng, Y. Su, J. Li, W. Tang, F. Yan, *Small Sci.* **2024**, *4*, 2300058.
[14] J. Li, D. Wu, Y. Yu, T. Li, K. Li, M.-M. Xiao, Y. Li, Z.-Y. Zhang, G.-J. Zhang, *Biosens. Bioelectron.* **2021**, *183*, 113206.
[15] J. Li, L. Tang, T. Li, K. Li, Y. Zhang, W. Ni, M.-M. Xiao, Y. Zhao, Z.-Y. Zhang, G.-J. Zhang, *ACS. Sens.* **2022**, *7*, 2680.
[16] Y. Wu, D. Ji, C. Dai, D. Kong, Y. Chen, L. Wang, M. Guo, Y. Liu, D. Wie, *Nano Lett.* **2022**, *22*, 3307.
[17] H. Yu, H. Zhang, J. Li, Z. Zhao, M. Deng, Z. Ren, Z. Li, C. Xue, M. G. Li, Z. Chen, *ACS. Sens.* **2022**, *7*, 3923.
[18] J. Song, H. Liu, Z. Zhao, P. Lin, F. Yan, *Adv. Mater.* **2024**, *36*, 2300034.
[19] K. Guo, S. Wustoni, A. Koklu, E. Díaz-Galicia, M. Moser, A. Hama, A. A. Alqahtani, A. N. Ahmad, F. S. Alhamlan, M. Shuaib, A. Pain, I. McCulloch, S. T. Arold, R. Grünberg, S. Inal, *Nat. Biomed. Eng.* **2021**, *5*, 666.
[20] A. Koklu, S. Wustoni, K. Guo, R. Silva, L. Salvigni, A. Hama, E. Diaz-Galicia, M. Moser, A. Marks, I. McCulloch, R. Grünberg, S. T. Arold, S. Inal, *Adv. Mater.* **2022**, *34*, 2202972.
[21] K. Ditte, T. A. N. Le, O. Ditzer, D. I. Sandoval Bojorquez, S. Chae, M. Bachmann, L. Baraban, F. Lissel, *ACS Biomater. Sci. Eng.* **2023**, *9*, 2140.

[22] S. Lai, M. Demelas, G. Casula, P. Cosseddu, M. Barbaro, A. Bonfiglio, *Adv. Mater.* **2013**, *25*, 103.
[23] S. Lai, M. Barbaro, A. Bonfiglio, *Sens. Actuat. B: Chem.* **2016**, *233*, 314.
[24] C. Napoli, S. Lai, A. Giannetti, S. Tombelli, F. Baldini, M. Barbaro, A. Bonfiglio, *Sensors* **2018**, *18*, 990.
[25] G. Casula, S. Lai, E. Loi, L. Moi, P. Zavattari, A. Bonfiglio, *Sens. Actuat. B: Chem.* **2024**, *398*, 134698.
[26] M. Demelas, S. Lai, A. Spanu, S. Martinoia, P. Cosseddu, M. Barbaro, A. Bonfiglio, *J. Mater. Chem. B* **2013**, *1*, 3811.
[27] D. F. Doyle, D. A. Braasch, C. G. Simmons, B. A. Janowski, D. R. Corey, *Biochem* **2001**, *40*, 53.
[28] S. Lai, P. Cosseddu, G. C. Gazzadi, M. Barbaro, A. Bonfiglio, *Org. Electron.* **2013**, *14*, 754.
[29] D. Inc, Standard protocols DNA shearing for Biorupt® Pico, https://www.diagenode.com/files/protocols/Standard_protocols_for_DNAShearing.pdf, (accessed: December **2020**).
[30] H. F. Iqbal, Q. Ai, K. J. Thorley, H. Chen, I. McCulloch, C. Risko, J. E. Anthony, O. D. Jurchescu, *Nat. Commun.* **2021**, *12*, 2352.